

Electronic Supplementary Information (ESI)

Nearly monodisperse PbS quantum dots for highly efficient solar cells: an in-situ seeded ion-exchange approach

Yan Dou,^a Ru Zhou,^{*a} Lei Wan,^a Haihong Niu,^a Juntian Zhou,^a Jinzhang Xu^a and Guozhong Cao^{*b}

^a School of Electrical Engineering and Automation, Hefei University of Technology, Hefei 230009, P.R. China. E-mail: zhouru@hfut.edu.cn

^b Department of Materials Science and Engineering, University of Washington, Seattle, WA 98195, USA. E-mail: gzcao@u.washington.edu

Experimental Section

Preparation of mesoporous TiO₂ films. The preparation of mesoporous TiO₂ films were performed by doctor-blading the prepared TiO₂ paste onto conducting F-doped tin oxide (FTO) glass substrates. The TiO₂ paste was obtained following a typical preparation procedure.¹ Specifically, a mixture of 0.5 g TiO₂ nanoparticles (Degussa P25), 0.25 g ethyl cellulose and 1.75 g α -terpineol was sonicated and stirred in 5.0 mL ethanol to form a slurry, with the resort to the evaporation of excess ethanol solutions. The TiO₂ paste was doctor-bladed onto pre-cleaned FTO substrates. For this step, a hole puncher was employed to punch the scotch tape spacer for controlling the active area of devices. Then a heat-treatment was further conducted in air at 500 °C for 30 min in a muffle furnace under a heating rate of 5 °C/min, resulting in the formation of mesoporous TiO₂ films.

IE deposition of PbS QDs. An IE approach was carried out to load PbS QDs upon TiO₂ films. The typical process is schematically illustrated in Fig. 1. Firstly, a chemical bath deposition (CBD) process allows the deposition of PbSO₃ seeds. Typically, 0.1 M Pb(CH₃COO)₂ (abbreviated as Pb(Ac)₂), 0.1 M Na₂SO₃, and 0.2 M N(CH₂COONa)₃ (abbreviated as Na₃NTA) aqueous solutions were prepared and

further mixed together to achieve precursor solutions following a volume ratio of 1:1:1. Then the TiO₂ films were immersed into the as-prepared precursor solution for 30 min at 24 °C in the dark. This step allows the deposition of PbSO₃ seeds onto TiO₂ nanoparticles. The films were taken out, thoroughly rinsed with deionized water and further dried undergoing air flow. Secondly, a further immersion of PbSO₃-seeded TiO₂ films into Na₂S solution enables the IE process occurred between PbSO₃ and S²⁻, producing PbS QDs onto TiO₂ films. The molar ratio of Na₂S solution referred herein was 0.1 M in methanol/water (v/v, 1/1) and the dip lasted for 2 min, followed by thorough rinsing with methanol and further drying. Furthermore, two SILAR cycles were carried out to prepare a ZnS passivation layer, by using 0.1 M Zn(Ac)₂ methanol solution and 0.1 M Na₂S methanol/water (v/v, 1/1) solution as the cationic and anionic precursor solutions. For the above-mentioned SILAR process, each dip lasted for 1 min. Furthermore, the devices with the CdS capping layers were also fabricated in this work. Four SILAR cycles were utilized to prepare the CdS layers directly capped onto PbS QDs, typically through alternatively dipping into 0.1 M Cd(Ac)₂ methanol solution and 0.1 M Na₂S methanol/water (v/v, 1/1) solution. In our experiments, the conventional SILAR processed PbS QD-sensitized films with and without the CdS capping layers were prepared as control samples for comparison. For the control samples, PbS QDs were loaded through four SILAR cycles by using 0.02 M Pb(Ac)₂ methanol solution and 0.02 M Na₂S methanol/water (v/v, 1/1) solution. The ZnS and CdS layers were also prepared through two and four SILAR cycles, respectively.

Assembly of solar cells. A sandwiched type QD-sensitized solar cell was constructed by sandwiching the photoanode and counter electrode with a scotch tape spacer, followed by permeating the assembly with the electrolyte.¹ In this work, the polysulfide electrolyte and Cu₂S counter electrode were employed. Specifically, the polysulfide electrolyte was obtained by dissolving 1 M S and 1 M Na₂S in deionized water. The Cu₂S counter electrode was prepared on the brass foil that was etched by the hydrochloric acid (mass fraction ~37.0%) at around 75 °C for 30 min and then immersed into the polysulfide electrolyte for 5 min, resulting in the formation of a

black Cu₂S layer on the foil.

Characterization of materials and devices. The morphology of samples was characterized by a scanning electron microscope (SEM, Philips XL30 FEG) and a transmission electron microscope (TEM, JEM-2100F). X-ray diffraction (XRD) spectra were collected on an X'Pert PRO MPD diffractometer by using Cu K α as the irradiation. X-ray photoelectron spectroscopy (XPS) was performed on an ESCALAB220Xi electron spectrometer (Thermo Scientific). UV-vis-NIR absorption spectra were achieved on an Agilent UV-vis-NIR spectrophotometer (CARY 5000) equipped with an integrating sphere accessory. Current density-voltage (J-V) measurements of solar cells were carried out under AM 1.5 illumination (One Sun, 100 mW cm⁻²) generated by a solar simulator (Oriel Sol 3A Solar Simulator, USA). The active area of devices was about 0.196 cm². Electrochemical impedance spectroscopy (EIS) was collected on a CHI660D electrochemical workstation. The explored frequency ranges from 10⁵ Hz to 0.1 Hz.

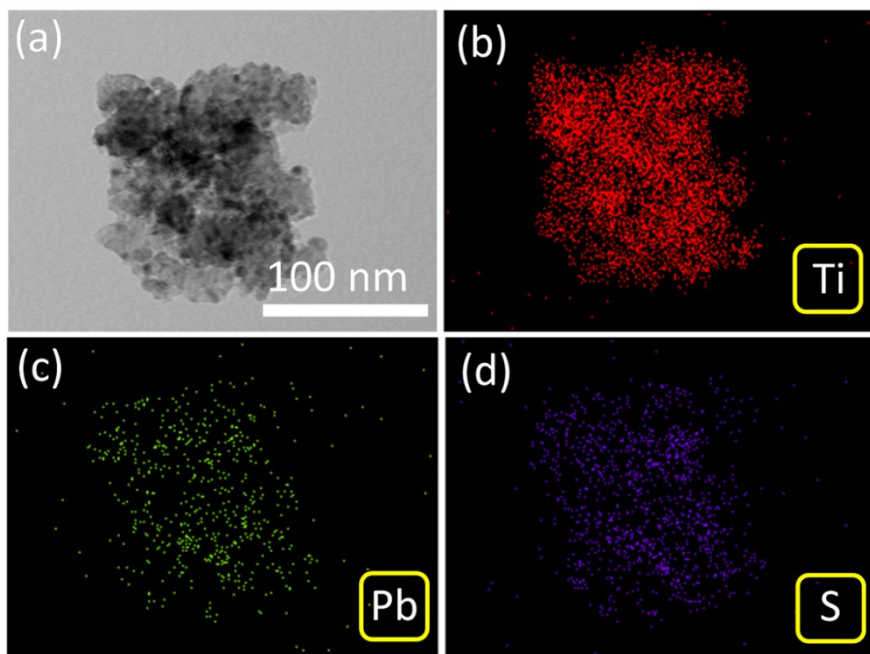


Fig. S1. (a) TEM images of IE processed PbS QD-deposited TiO₂ nanoparticles, and the corresponding mapping images showing the spatial elemental distribution of (b) Ti, (c) Pb, and (d) S, respectively.

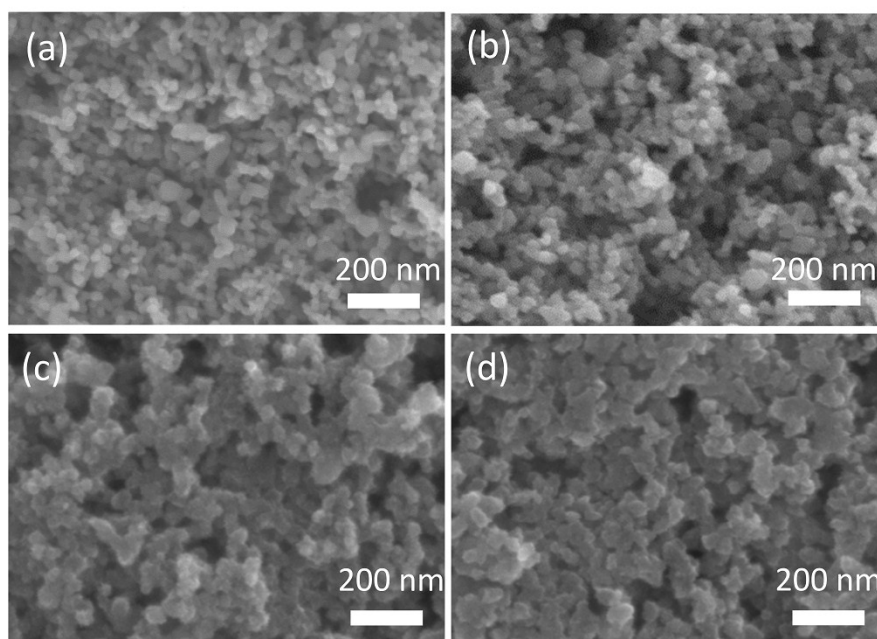


Fig.S2. Top-view SEM images of (a) bare, (b) PbSO₃ seeded, and (c) IE and (d) SILAR processed PbS QDs deposited mesoporous TiO₂ films.

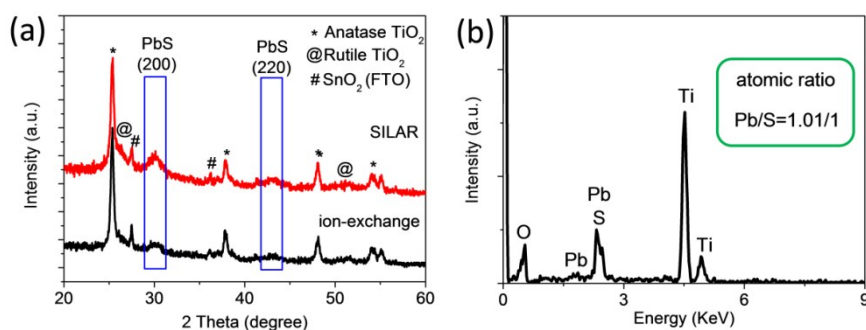


Fig. S3. (a) XRD patterns of IE and SILAR processed PbS QD-sensitized TiO₂ films. (b) EDX spectrum of IE processed PbS QD-sensitized TiO₂ films.

Table S1. Absorption onset and effective bandgap (E_g) of IE and SILAR processed PbS QDs, and corresponding bandgap blue shift (ΔE) with respect to that of bulk PbS (0.41 eV).

sample	absorption onset (nm)	E_g (eV)	ΔE (eV)
IE	867	1.43	1.02
SILAR	1138	1.09	0.68

Estimation of Effective Bandgaps and Absorption Onsets

The effective bandgaps of PbS QDs processed by different approaches can be estimated by using eqn (1), which describes the relationship between the bandgap (E_g) for direct interband transition and the absorption coefficient (A) near the absorption edge:¹

$$(Ah\nu)^2 = c(h\nu - E_g) \quad (1)$$

where ν is the frequency, h is Planck constant and c is a constant. By extrapolating the linear portion of the $(Ah\nu)^2$ versus $h\nu$ plots at $A=0$, as performed in Fig. 3b, the estimated effective bandgaps and absorption onsets are summarized in Table S1.

Table S2. Photovoltaic parameters of IE and SILAR processed PbS QDSCs, measured under the illumination of One Sun (AM 1.5, 100 mW cm⁻²).

Device	J_{sc} (mA/cm ²)	V_{oc} (V)	FF	PCE (%)
IE-PbS	8.73	0.43	0.34	1.30
SILAR-PbS	2.26	0.07	0.21	0.03
IE-PbS/CdS	14.30	0.437	0.482	3.01
SILAR-PbS/CdS	14.59	0.425	0.401	2.48

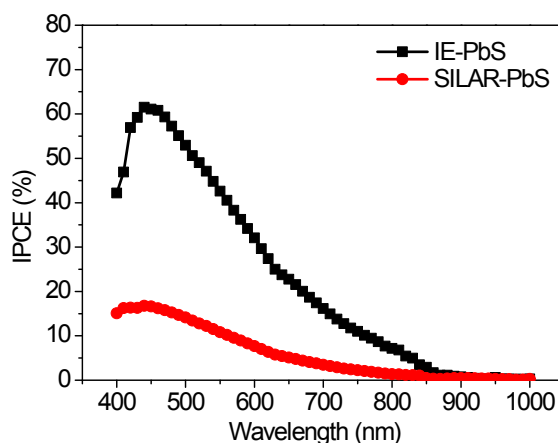


Fig. S4. IPCE spectra of IE and SILAR processed PbS QDSCs.

Optical and Electrochemical Examinations of CdS-capped PbS

QDSCs

Fig. S5a shows the UV-vis-NIR absorption spectra of IE and SILAR processed PbS/CdS QD-sensitized TiO₂ photoanodes. Both spectra were similar to the absorption spectra of PbS QD-sensitized TiO₂ films as given in Fig. 3a, except the observation of the obvious humps at around 480 nm which correspond to the absorption edge of CdS. As we know, the critical factors that determine the photovoltaic performance of QDSCs include light harvesting, electron injection and charge collection.^{2,3} As the light harvesting capability of IE processed photoanode has been shown to be lower than that of the SILAR processed one, it is reasonable to speculate that the efficiencies of electron injection and/or collection that followed by photocarrier generation are much more efficient in an IE processed device in view of its more superior photovoltaic performance. The higher CB of IE processed QDs are expected to contribute to more efficient electron injection while the evaluation of electron collection requires further characterization. The electrochemistry impedance measurements were performed to evaluate the interfacial charge recombination processes in solar cells. The Nyquist plots of impedance spectra for IE and SILAR processed PbS QDSCs with the CdS capping layer are presented in Fig. S5b, recorded under dark condition at an applied forward bias of -0.50 V. As shown, both Nyquist plots show two semicircles. The contact series resistance (R_s), determined by the starting point of the curve, mainly corresponds to the sheet resistance of conducting substrates and contact resistance between substrates and TiO₂. The small semicircle (R_1) and large semicircle (R_2), responded upon high-frequency and intermediate-frequency ranges, are associated with the resistance of the redox reaction at the interface of counter electrode/electrolyte and the charge recombination resistance at the TiO₂/QD/electrolyte interface, respectively.² The curves were fitted by using

the equivalent circuit as given in the inset of Fig. S5b. The results show that R_1 demonstrates no obvious resistance differences for both devices, owing to the use of identical polysulfide electrolyte and Cu_2S counter electrode. We pay special attention to the striking difference of the recombination resistance R_2 between both devices. The R_2 of the IE processed device is fitted to be around 39Ω , which is larger than that of 31Ω for the control SILAR processed device. Since the larger R_2 indicates a lower recombination rate in solar cells, the photogenerated carriers transported in IE processed photoanodes should be much more difficult to recombine with the redox couple of $\text{S}^{2-}/\text{S}_n^{2-}$ in the electrolyte in contrast to the SILAR processed photoanodes. The impedance results are further evidenced by the J-V characteristics measured under dark conditions as given in Fig. S5c, which demonstrates a smaller dark current for the IE processed device in contrast to the conventional SILAR processed one. In addition, the stability test of devices measured at interval time (Fig. S5d) reveals that the IE processed device ensures better device stability than that of the SILAR processed one, probably arising from the retarded charge recombination. Considering that other components including TiO_2 film, electrolyte and counter electrode are identical in this work, the different charge recombination should involve with the features of QDs.² Specifically, the nearly monodisperse QDs prepared by the IE strategy might contribute to the promoted charge transfer and retarded charge recombination. That is, in comparison with the SILAR approach, the IE processed device affords larger recombination resistance that allows more effective suppression of recombination, thereby further boosting the electron collection efficiency.

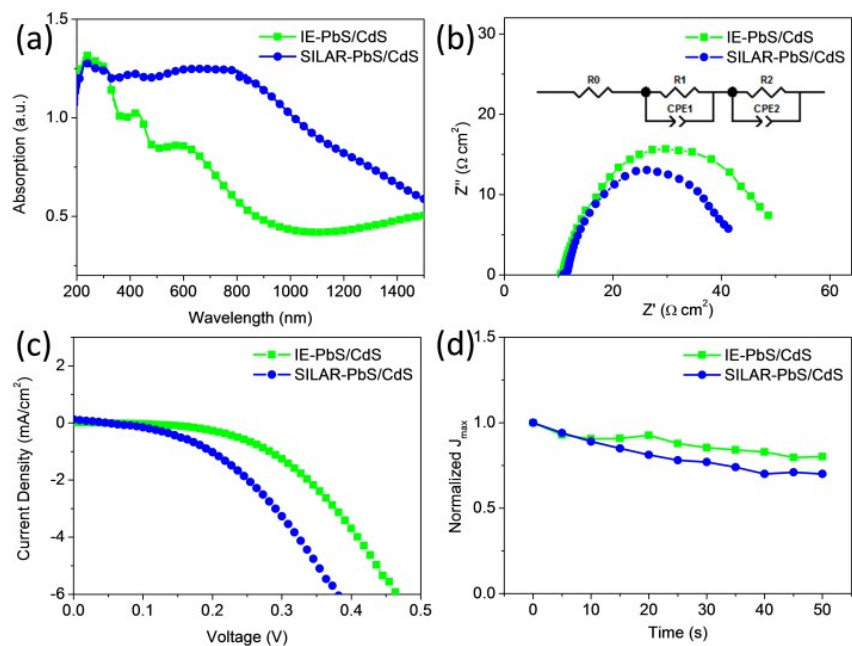


Fig. S5. (a) UV-vis-NIR absorption spectra of IE and SILAR processed PbS/CdS QD-sensitized TiO_2 photoanodes, and (b) Nyquist plots of impedance spectra recorded under dark condition at an applied forward bias of -0.50 V (the inset shows the corresponding equivalent circuit), (c) Current density-voltage (J-V) characteristics measured under dark conditions, and (d) Stability test for IE and SILAR processed PbS QDSCs with the CdS capping layer.

References

1. R. Zhou, Q. F. Zhang, J. J. Tian, D. Myers, M. Yin and G. Z. Cao, *J Phys Chem C*, 2013, **117**, 26948-26956.
2. R. Zhou, J. Xu, F. Huang, F. W. Ji, L. Wan, H. H. Niu, X. L. Mao, J. Z. Xu and G. Z. Cao, *Nano Energy*, 2016, **30**, 559-569.
3. P. V. Kamat, *Accounts Chem Res*, 2012, **45**, 1906-1915.